



Surrounding rock effect on coal burst under unloading condition: a numerical study

Yuezong Yang¹ · Zhennan Zhang¹

Received: 17 March 2021 / Accepted: 22 July 2021 / Published online: 12 August 2021
© Saudi Society for Geosciences 2021

Abstract

In the coal burst induced by excavation, the burst body is not a closed system because the surrounding rock (the roof and the floor) can work on it. In order to investigate the surrounding rock effect on coal burst caused by unloading, the discretized virtual internal bond is employed to comprehensively simulate the burst process of the rock-coal-rock (RCR) body. The simulation results suggest that there exists a critical in situ stress, which is about 0.7 times of the uniaxial compression strength of RCR. When the in situ stress exceeds this critical value, the unloading can induce the RCR burst. There also exists a critical surrounding rock stiffness, which is about 8.0 times of the coal stiffness. When the surrounding rock stiffness is smaller than this critical value, it has significant impact on the coal burst while when it exceeds the critical value, it has almost no effect on unloading burst. The characteristic surrounding rock size, over which the surrounding rock has no effect on the burst, is about 4.0 times of the coal seam. Besides these, some quantitative regularities of acoustic emission during coal burst have been obtained. These findings are helpful to improve the understanding on coal burst. They provide valuable references for the prediction of coal burst.

Keywords Coal burst; · Dynamic fracture; · Unloading; · Numerical simulation; · Discretized virtual internal bond

Introduction

The coal burst is a violent failure process induced by unloading the coal seam which had been subjected to the high in-situ stresses. During the unloading process, the energy stored in the coal seam and surrounding rock release rapidly, usually leading to rock burst. In order to predict the occurrence of such disaster, it is quite necessary to understand the underlying physical mechanism of coal burst. Many factors can trigger the coal burst, e.g., the dynamic load (Lu et al. 2020; Zhou et al. 2020), the cycling load (Zhang et al. 2020; Gong et al. 2021) and the unloading (Si and Gong 2020; He et al. 2021). In this paper, we are focused on the unloading-induced coal burst. The existed studies, e.g., Chen et al. 2013, Yin et al. 2015, Zhu et al. 2019, suggest that the unloading value, unloading rate and stress state have significant impact on the

coal burst. However, the coal seam is not a closed system during coal burst since the surrounding rock works on it. It should be more reasonable to take the burst body and surrounding rock as a whole to study the coal burst mechanism. To study the surrounding rock effect, some scholars took the combined coal and rock as samples in experimental study. Liu et al. (2015) suggested that the combined coal-rock sample strength mainly depends on the strength of coal rather than rock. With the coal-rock height ratio increasing, the combined sample strength decreases (Liu et al. 2018). The failure of the coal-rock sample is mainly induced by the failure of coal component (Zuo et al. 2013; Yao et al. 2020). The larger height ratio of rock to coal makes the impact tendency higher (Song et al. 2021). These studies reveal the interaction mechanisms between the coal and the rock in the coal burst. Although a great progress has been achieved along this line, the unloading effect has not been considered yet.

To comprehensively consider the surrounding rock and the unloading effect is a very tough problem in experiment. In such situation, the numerical simulation provides a feasible approach to this problem. So far, some numerical methods have been used to simulate the rock burst or coal burst, e.g., the continuum finite

Responsible Editor: Murat Karakus

✉ Zhennan Zhang
zhennanzhang@sjtu.edu.cn

¹ School of Naval Architecture, Ocean and Civil Engineering, Shanghai Jiao Tong University, Shanghai 200240, China

element method (Tao et al. 2012; Manouchehrian and Cai 2016), the discrete element method (Yardimci and Karakus 2020; Song et al. 2020). In this paper, we will use the discretized virtual internal bond (DVIB) method (Zhang 2013) to explore the coal burst. The reason to choose DVIB is that DVIB can represent the mesostructural characteristics of rock. It can directly simulate the dynamic fracture process in the large displacement and large deformation cases without any explicit fracture criterion.

Method

Rock consists of mineral grains on the meso scale. In DVIB (Zhang 2013). Each mineral grain can be treated as discrete bond cell, which is composed of finite number of bonds, shown in Fig. 1. The strain energy of a bond cell is

$$W = \sum \Phi(l) \tag{1}$$

where Φ is the bond potential; l is the bond length.

The force vector of the bond cell is derived as

$$F_i = \frac{\partial W}{\partial u_i} = \sum \Phi'(l) \frac{\partial l}{\partial u_i} \tag{2}$$

and the stiffness matrix is

$$K_{ij} = \frac{\partial^2 W}{\partial u_i \partial u_j} = \sum \left[\Phi''(l) \frac{\partial l}{\partial u_i} \cdot \frac{\partial l}{\partial u_j} + \Phi'(l) \frac{\partial^2 l}{\partial u_i \partial u_j} \right] \tag{3}$$

where u_i is the component of the nodal displacement vector; $\Phi'(l)$ and $\Phi''(l)$ denote the first and the second derivative of $\Phi(l)$ with respect to the bond length l , respectively.

Considering that the rock is a quasi-brittle material, the elastobrittle bond potential is adopted, whose first derivative with respect to bond length is

$$\Phi'(l) = \begin{cases} k_e(l-l_0) & l \leq l_f & \text{Elastic} \\ 0 & l > l_f & \text{Failure} \end{cases} \tag{4}$$

where l_0 is the undeformed bond length; l_f the failure bond length, $l_f = l_0(1 + \varepsilon_f)$, ε_f is the failure bond strain; k_e the initial elastic stiffness of bond.

$$k_e = \lambda \cdot \frac{EV}{\Omega l_0^2} \tag{5}$$

where E is the Young's modulus of material; V is the volume of a bond cell; Ω is the bond number in a bond cell; λ is a coefficient, $\lambda=6$ for the 3D, $\lambda=3$ for the plane-stress, and $\lambda=3.2$ for the plane-strain cases, respectively.

Usually, there exists an interface between the coal seam and the rock layer, shown in Fig. 2a. To describe the interface between the coal seam and rock layer, we use the following bond potential (Gao and Klein 1998) to characterize the bond cell array (Fig. 2b) along the coal-rock interface.

$$F_b = k_e \cdot (l-l_0) \cdot \exp\left(-\frac{l-l_0}{\varepsilon_p l_0}\right) \tag{6}$$

where ε_p is the peak force bond strain of interface.

Considering the computation efficiency, we use the implicit time-integration algorithm for the initial stress field while use the explicit algorithm for the coal burst process after unloading.

Verification and calibration

To verify the DVIB, the following two tests are simulated, namely the uniaxial compression of RCR and the unloading failure of coal sample. The uniaxial compressive sample of RCR is shown in Fig. 2a. Its height and width are 100mm and 50mm, respectively. The uniaxial compression tests of the rock, the coal and RCR are firstly simulated to calibrate the parameters, which are

Rock: $E_R=12.85\text{GPa}$, $\rho_R=2700\text{kg/m}^3$, $\varepsilon_{fR}=7.82 \times 10^{-3}$;

Coal: $E_C=2.59\text{GPa}$, $\rho_C=1328\text{kg/m}^3$, $\varepsilon_{fC}=6.20 \times 10^{-3}$;

Coal-rock interface: $E_{Int}=2.15\text{GPa}$, $\rho_{Int}=2014\text{kg/m}^3$, $\varepsilon_{pInt}=4.12 \times 10^{-3}$.

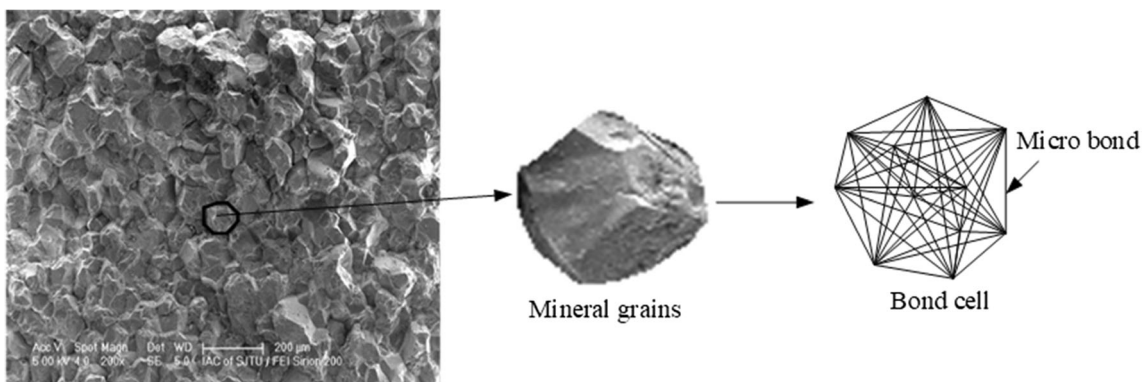


Fig. 1 Modeling rock with DVIB

Fig. 2 RCR samples for uniaxial compression test **a** RCR sample, **b** meshing scheme

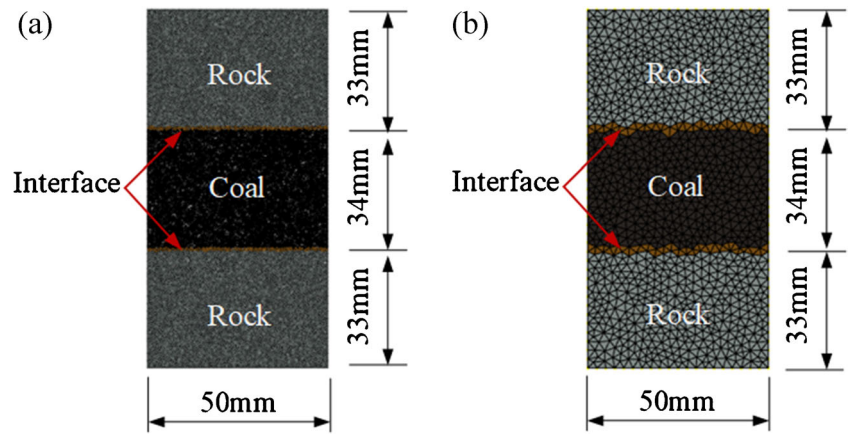
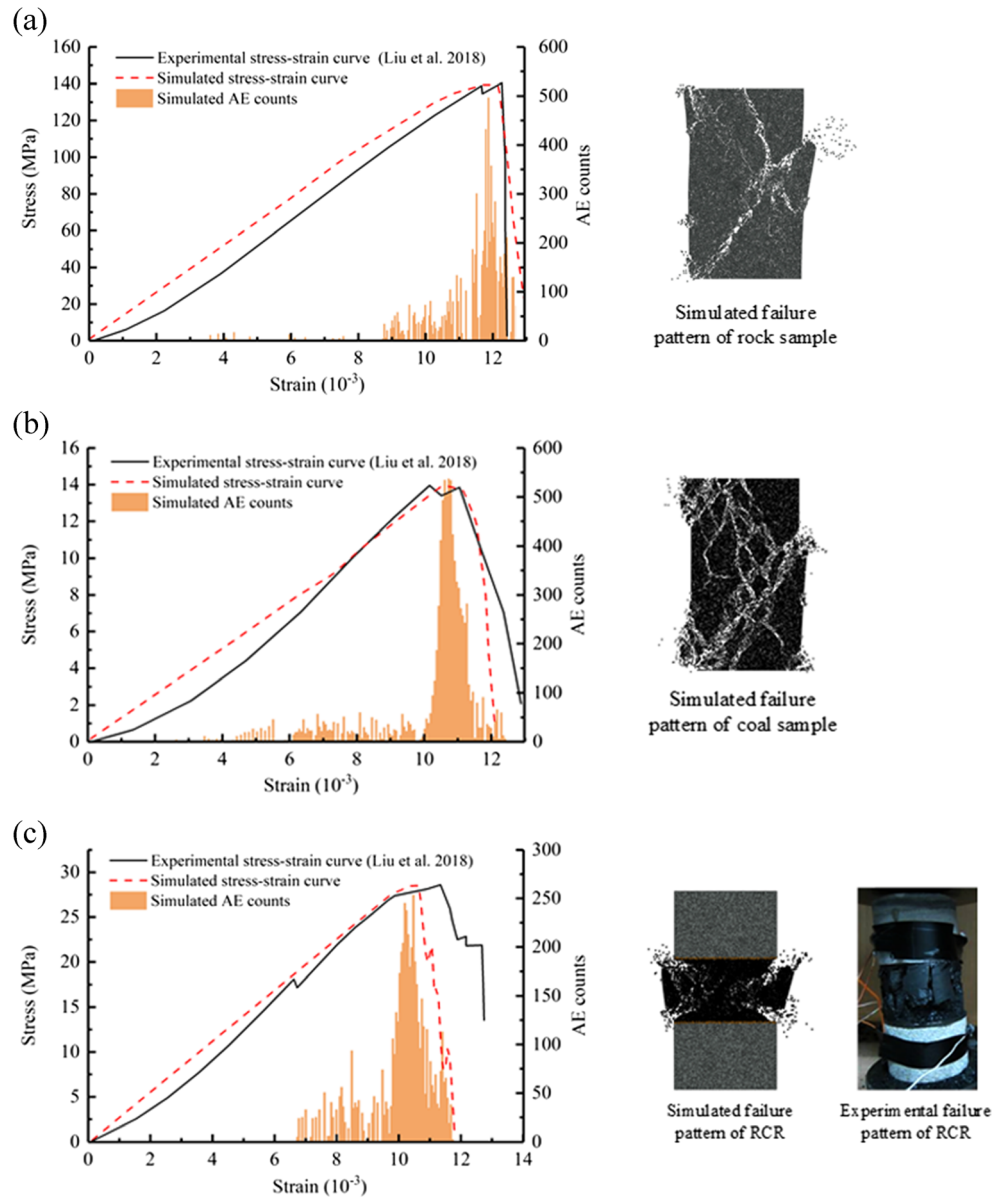


Fig. 3 Comparison between the simulated and the experimental results (Liu et al. 2018) of uniaxial compression test **a** rock sample, **b** coal sample, **c** RCR sample



With these calibrated parameters, the simulation results are shown in Fig. 3. The simulated stress-strain curves well match the tested one (Liu et al. 2018). In the failure process of samples, the acoustic emission (AE) signal is the elastic wave induced by the micro crack initiation. One bond rupture indicates one micro crack initiation. So, it is reasonable that the number of broken bonds is recorded as the AE counts. From the simulated results it is seen that there are few AE counts at the initial loading stage. With the stress approaching to the peak value, the AE count increases sharply. This is consistent with the experimental observation (Liu et al. 2018). The crack pattern of coal (Fig. 3b) is more complicated than the rock (Fig. 3a). In RCR (Fig. 3c), the failure mainly occurs in the coal section. The simulated results show that the DVIB model can simulate the failure of rock, coal and their combination.

The dimensions and boundary condition of the simulated object for unloading test (Zhu et al. 2019) is shown in Fig. 4a. The calibrated parameters above are adopted. The simulated coal burst pattern (Fig. 4b) is mainly the lamination near the unloading face, which is consistent with experimental observation (Fig. 4c). So, it is feasible to adopt the DVIB model to simulate unloading failure of coal.

Coal burst simulation

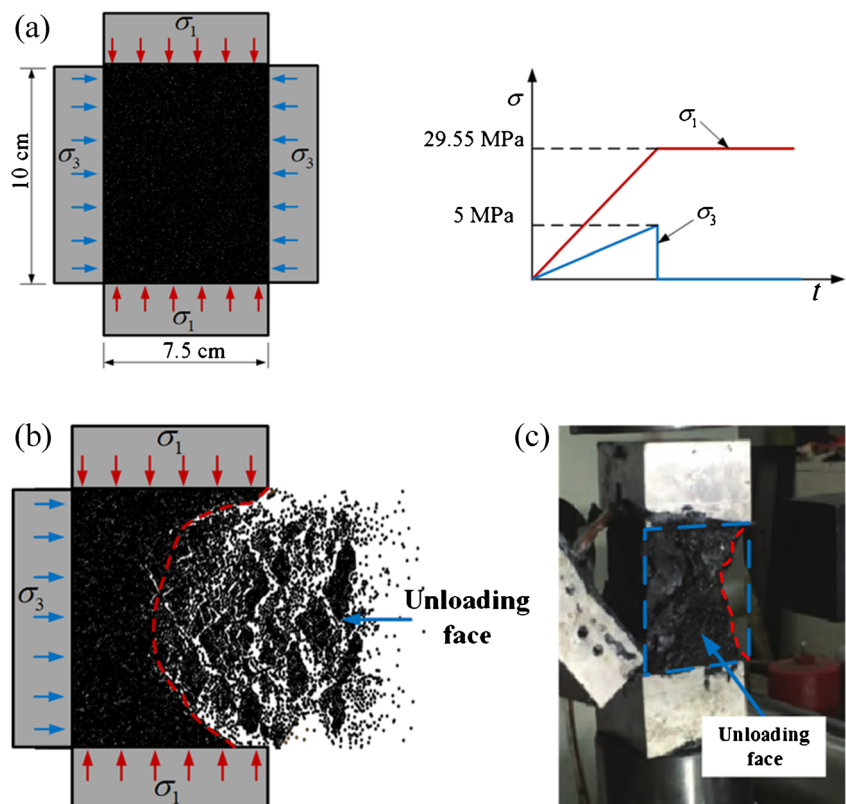
Simulation model

Under the same in situ stress, different surrounding rock stores different amounts of strain energy, which may lead to different failure patterns of coal seam after excavation. A simplified geological model is shown in Fig. 5a. There are three strata, namely the roof, coal seam and floor. Correspondingly, the computation object is shown in Fig. 5b. The height and the mechanical properties of the roof are the same as the floor. The calibrated parameters of rock, coal, and coal-rock interface in above are adopted. Firstly, the vertical compressive stress is applied on the top of this sample with the other boundaries normally restricted. When the vertical stress σ_1 reaches the prescribed value, the top boundary is normally restricted. Next, the normal restriction applied on the right lateral side of coal section is abruptly removed to simulate excavation.

Effect of in situ stress

The in situ stress is an important factor impacting coal burst. To explore the in situ stress effect on coal burst, we set the sample dimensions $L=h_C=h_R=10\text{cm}$. By using the calibrated

Fig. 4 Comparison between the simulated unloading failure pattern of coal sample and the experimental result (Zhu et al. 2019) **a** dimensions and boundary condition of simulated object, **b** simulated failure pattern, **c** experimental failure pattern



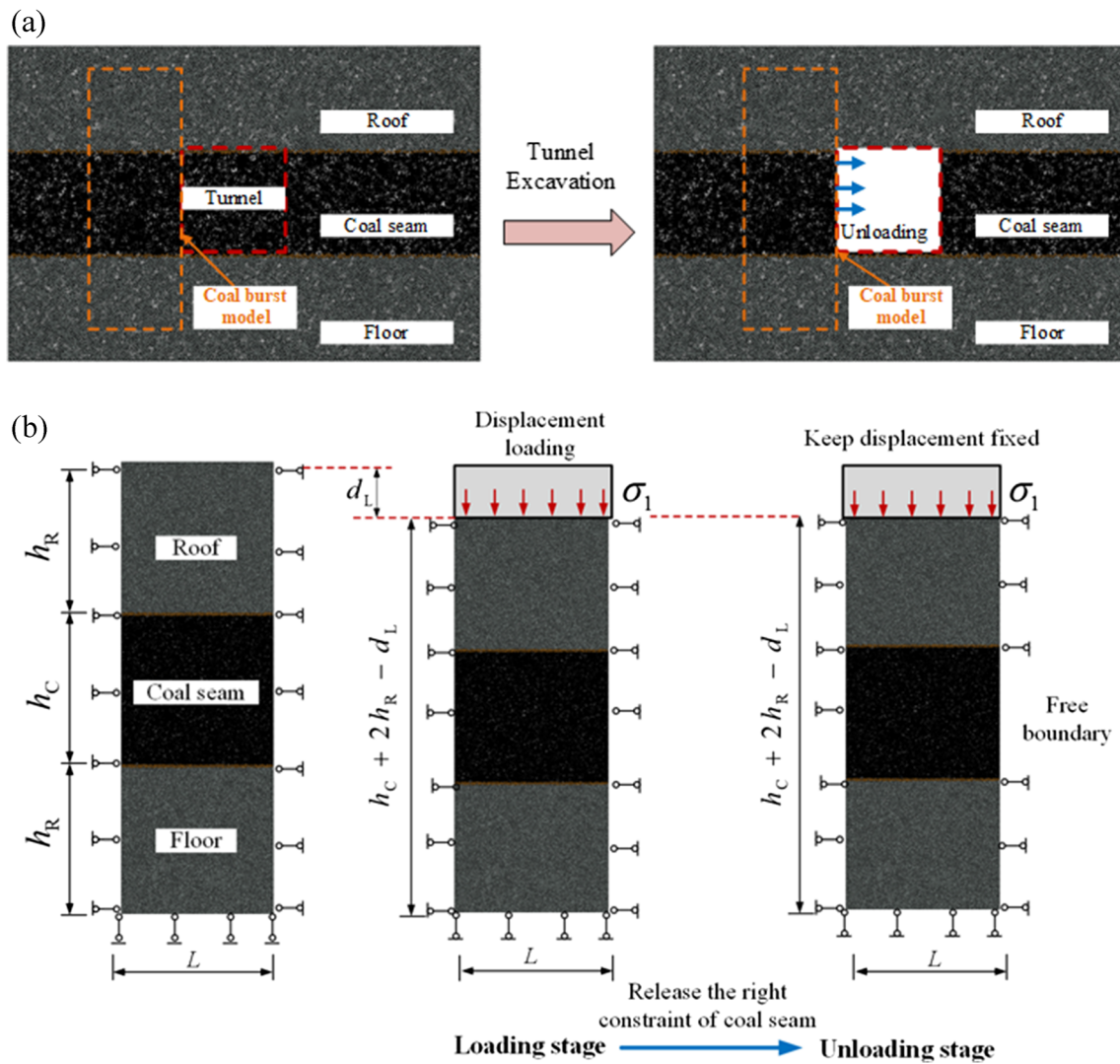


Fig. 5 Simulation setup of coal burst model a excavation in coal mining, b coal burst model

parameters above, the uniaxial compression strength (UCS) of RCR sample is 24.82MPa. A normalized stress $\bar{\sigma}_i$ is defined by $\bar{\sigma}_i = \sigma_i / \text{UCS}$ to represent the in situ stress. We set 8 cases with different initial in situ stresses, namely $\bar{\sigma}_i = 0.5, 0.6, 0.7, 0.8, 0.9, 1, 1.5$ and 2 .

Figure 6 shows the simulation results. It is found that there is a critical in situ stress of unloading failure, which is about 0.7 times of UCS. When the initial in situ stress is smaller than this critical one, the unloading failure does not occur. In the case of $\bar{\sigma}_i = 0.7$, the vertical stress does not decrease (Fig. 6a) and no AE counts are monitored (Fig. 6b). When the initial in situ stress exceeds this critical value, the unloading triggers the coal seam failure. With the initial in situ stress increasing, the vertical stress decreases faster (Fig. 6a) and more AEs are released (Fig. 6b). According to these data, the relationship between the final AE counts and the initial in situ stress (shown as Fig. 6c) is obtained by regression:

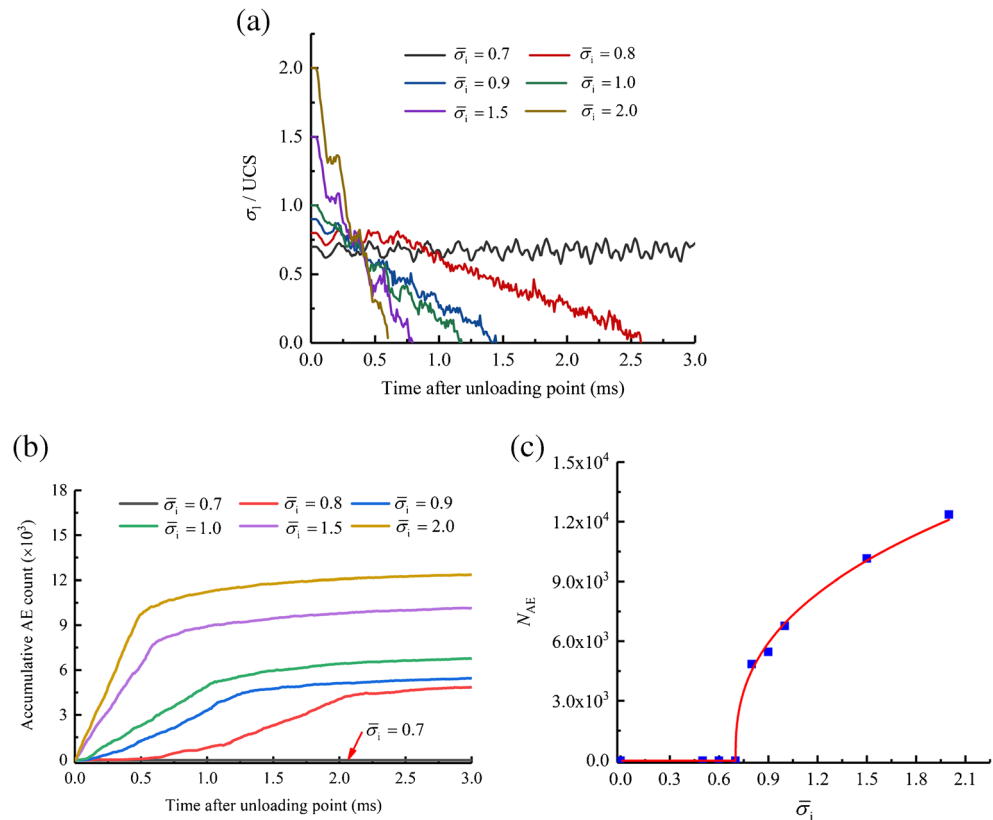
$$N_{AE} = \begin{cases} 0 & \bar{\sigma}_i \leq \bar{\sigma}_c \\ A \times (\bar{\sigma}_i - \bar{\sigma}_c)^\alpha & \bar{\sigma}_i > \bar{\sigma}_c \end{cases} \quad (7)$$

where N_{AE} is the final AE counts; A and α are the fitting parameters; $\bar{\sigma}_c$ is the critical in situ stress. For the RCR with the calibrated material parameters, $\bar{\sigma}_c = 0.7, A = 10940.75$ and $\alpha = 0.383$.

The simulated unloading burst process of RCR in the case of $\bar{\sigma}_i = 1$ is shown in Fig. 7. The main characteristics of coal burst observed in experiments (He et al. 2012) are reproduced in that firstly some small grains eject, then some big fragments fall down and next many eject.

To verify the relationship between the final AE counts and the initial in situ stress, more cases are studied. At first, we keep the modulus ratio fixed, but change the absolute modulus value of rock and coal. For the larger modulus case, $E_R/E_C =$

Fig. 6 Stress evolution and AE of the cases with different initial in situ stresses **a** vertical stress evolution, **b** AE evolution, **c** relation between final AE counts and initial in situ stresses



19.28GPa/3.89GPa, the UCS is 37.27MPa. For the smaller modulus case, $E_R/E_C= 6.43GPa/1.30GPa$, the UCS is 12.46MPa. Then we re-simulate this problem. The simulation results are shown in Fig. 8a. The standard case is the one with the calibrated parameters. It shows that the critical in situ stress of unloading failure is still about 0.7 times of UCS. When the in situ stress is lower than the critical value, the coal burst does not occur. When the in situ stress exceeds the critical value, the relationship between the final AE counts and the initial in situ stress follows the power function (Eq. (7)).

This suggests that the relationship of Eq. (7) holds in the cases of different elastic modulus. Then, we simulate this problem with different bond failure strains. In the larger bond failure strain case, $\epsilon_{FR}/\epsilon_{FC}/\epsilon_{pInt}=11.73\times 10^{-3}/9.30\times 10^{-3}/6.18\times 10^{-3}$, the UCS is 37.19MPa. In the smaller bond failure strain case, $\epsilon_{FR}/\epsilon_{FC}/\epsilon_{pInt}=3.91\times 10^{-3}/3.10\times 10^{-3}/2.06\times 10^{-3}$, the UCS is 12.52MPa. The simulated results (Fig. 8b) show that the bond failure strains almost have no influence on the relationship between the final AE counts and the initial in situ stress.

Fig. 7 Unloading failure process of RCR in the case of $\bar{\sigma}_i = 1$ (t is the time after unloading point)

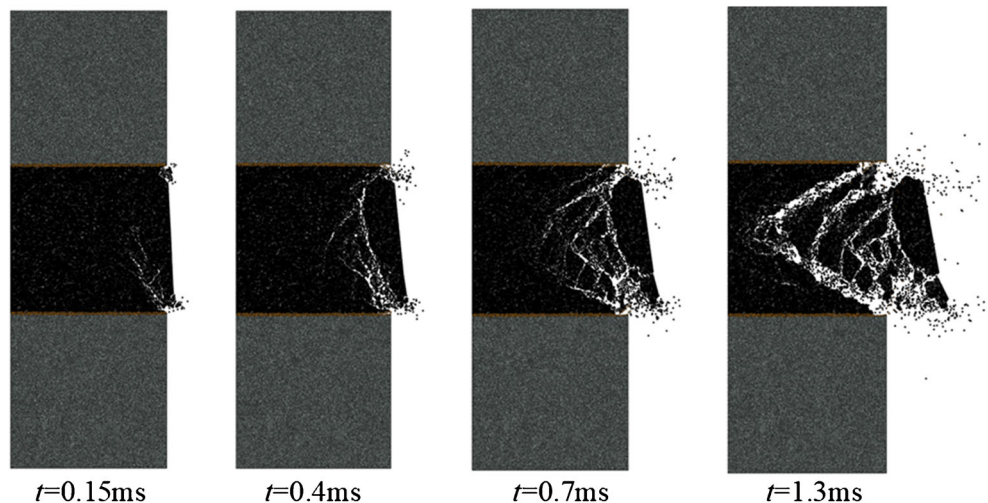
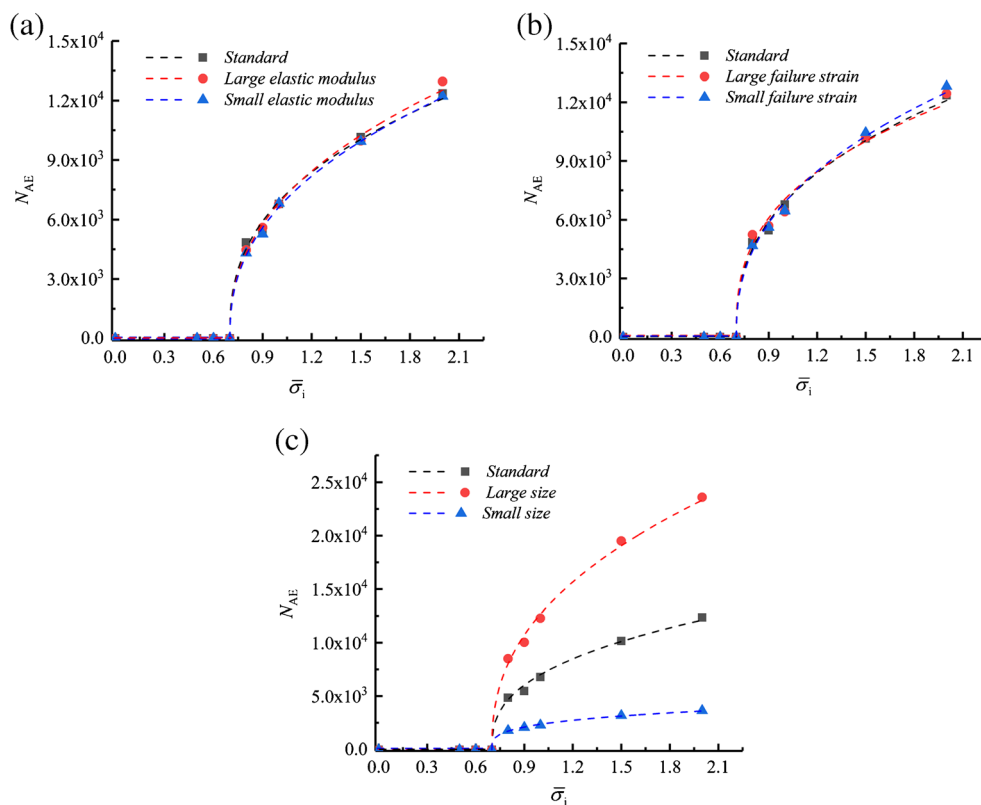


Fig. 8 Relation between final AE counts and initial in situ stresses for the samples with different **a** elastic moduli, **b** bond failure strains, **c** sample sizes



Next, we simulate this problem with different sample size. For the larger sample size case, $L=h_C=h_R=15\text{cm}$, the UCS is 22.89MPa. For smaller one, $L=h_C=h_R=5\text{cm}$, the UCS is 27.47MPa. The same variation trend can be found, but the regression coefficients are different. The detailed fitting parameters are listed in Table 1.

Effect of surrounding rock stiffness

To study the effect of surrounding rock stiffness on the coal burst, we set 6 cases of surrounding rock stiffness, namely $E_R/E_C=1, 2, 4, 8, 12$ and 16 , in which E_C is fixed, i.e., $E_C=2.59\text{GPa}$ and $\bar{\sigma}_i=1, L=h_C=h_R=10\text{cm}$.

The simulated results show that there is a critical surrounding rock stiffness ratio, which is about E_R/E_C

$E_C=8.0$. As shown in Fig. 9a, when the surrounding rock stiffness is smaller than the critical value, with the increase of surrounding rock stiffness, both the AE growth rate and accumulative AE counts decrease. While the surrounding rock stiffness exceeds this critical value, both the AE growth rates and accumulative AE counts tend to be constant. The relationship between the final AE counts and surrounding rock stiffnesses (Fig. 9b) satisfies

$$N_{AE} = P + Q \times \exp\left(-\frac{E_R/E_C}{\beta}\right) \tag{8}$$

where $P, Q,$ and β are fitting parameters.

To verify the relationship between the final AE counts and the surrounding rock stiffnesses, more cases are studied. The

Table 1 Fitting parameters for the relation between final AE counts and initial in situ stresses

Sample	$\bar{\sigma}_c$	A	α
Standard	0.70	10940.75	0.373
Large elastic modulus	0.70	11237.99	0.414
Small elastic modulus	0.70	10908.36	0.415
Large failure strain	0.70	10844.39	0.370
Small failure strain	0.70	11247.59	0.407
Large size	0.69	20905.30	0.416
Small size	0.70	3336.08	0.383

Fig. 9 AE of the cases with different surrounding rock stiffnesses **a** AE evolution, **b** relation between final AE counts and surrounding rock stiffnesses

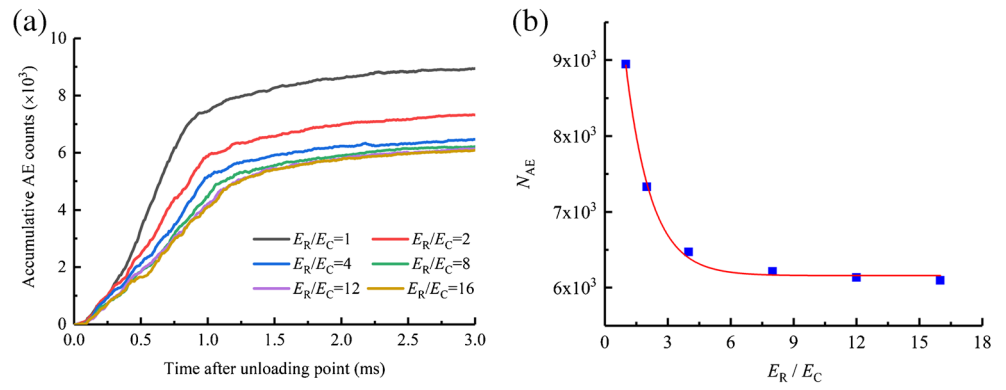


Table 2 Fitting parameters for the relation between final AE counts and surrounding rock stiffnesses

Sample	P	Q	β
Standard	6158.42	6308.69	1.216
Large elastic modulus	6126.12	6300.79	1.307
Small elastic modulus	6149.27	5497.65	1.368
Large failure strain	6154.22	5913.41	1.363
Small failure strain	6072.53	5716.78	1.333
Large size	11758.21	11881.50	1.287
Small size	1867.99	2039.53	1.350

Fig. 10 Relation between final AE counts and surrounding rock stiffnesses for the samples with different **a** elastic moduli, **b** bond failure strains, **c** sample sizes

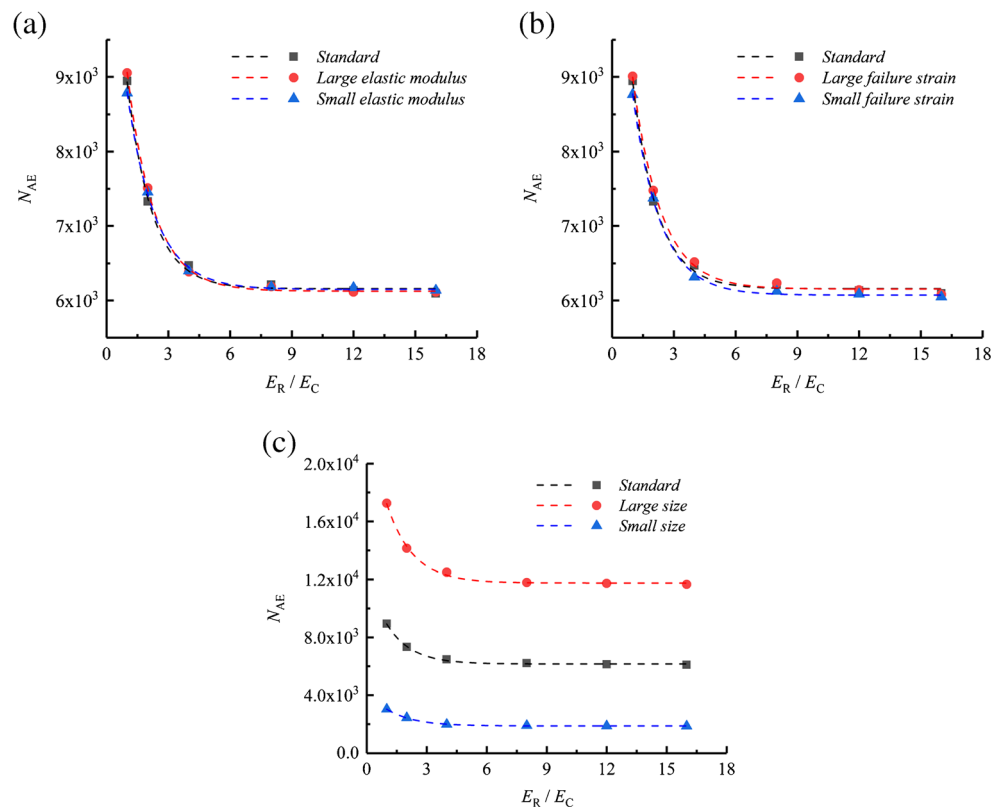
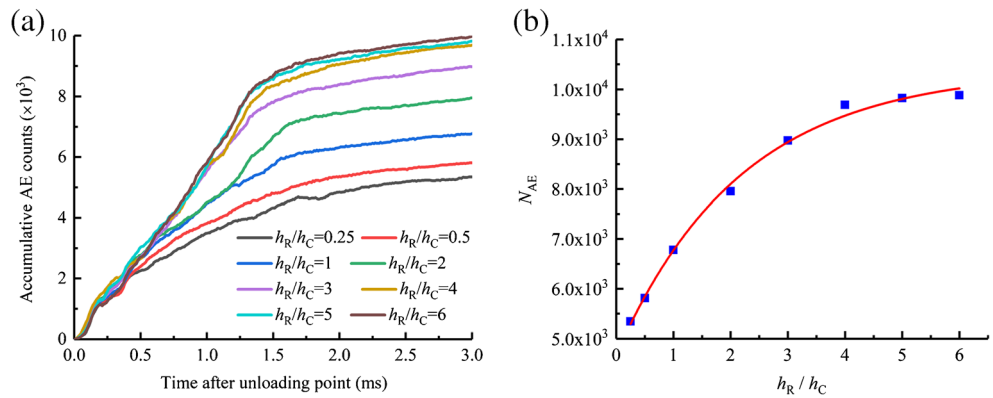


Fig. 11 AE of the cases with different surrounding rock sizes **a** AE evolution, **b** relation between final AE counts and surrounding rock sizes



simulated results show that for the cases of different material elastic moduli (Fig. 10a) and bond failure strains (Fig. 10b), the AE regularities are almost the same. For the samples with different sizes, as shown in Fig. 10c, the AE regularities all follow the exponential function, i.e., Eq. (8). The detailed fitting parameters for the different cases are listed in Table 2.

Effect of surrounding rock size

In the analysis of tunnel excavation, the reasonable evaluation of surrounding rock size is an important issue. To investigate

the effect of surrounding rock size, we set 8 cases, namely $h_R/h_C = 0.25, 0.5, 1, 2, 3, 4, 5,$ and 6 , in which h_C is fixed, i.e., $h_C = 10\text{cm}$. The calibrated material parameters and the same initial in situ stress, $\bar{\sigma}_i = 1$, are adopted in these cases.

The simulated results (Fig. 11) show that there is a critical surrounding rock size, which is about $h_R/h_C = 4.0$. With the surrounding rock size approaching to the critical value, the AE count also approaches to a limit value. So, when the surrounding rock size exceeds a critical size, the increase of surrounding rock size has almost no influence on unloading failure. The relation between the final AE counts and the surrounding rock sizes satisfies the following functional relation:

Fig. 12 Relation between final AE counts and surrounding rock sizes for the samples with different **a** elastic moduli, **b** bond failure strains, **c** sample sizes

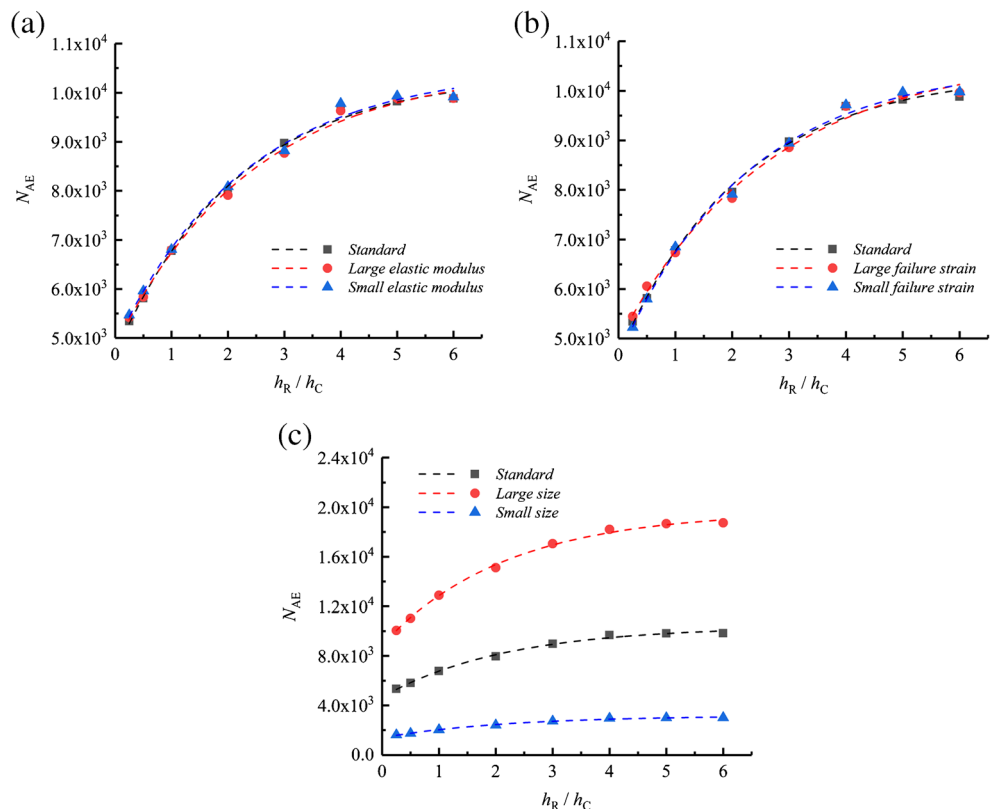


Table 3 Fitting parameters for the relation between final AE counts and surrounding rock sizes

Sample	M	N	γ
<i>Standard</i>	10388.69	5715.60	2.184
<i>Large elastic modulus</i>	10533.95	5706.10	2.447
<i>Small elastic modulus</i>	10516.62	5656.37	2.324
<i>Large failure strain</i>	10737.55	5777.54	2.665
<i>Small failure strain</i>	10538.23	5915.93	2.258
<i>Large size</i>	19670.92	10773.67	2.182
<i>Small size</i>	3176.66	1785.47	2.226

$$N_{AE} = M - N \times \exp\left(-\frac{h_R/h_C}{\gamma}\right) \quad (9)$$

where M , N , and γ are fitting parameters.

To verify the relation between the final AE counts and the surrounding rock sizes, more cases are studied. The simulated results (Fig. 12) show that the AE regularities of surrounding rock size do not change with the material elastic moduli (Fig. 12a) and bond failure strains (Fig. 12b). Figure 12c suggests that for the samples with different sizes, all the AE regularities follow the exponential function, i.e., Eq. (9). The detailed fitting parameters for the different cases are listed in Table 3.

Conclusions

A series of coal burst simulations with consideration of the surrounding rock and the unloading effect are conducted by using DVIB. The influence of in situ stress, surrounding rock stiffness and surrounding rock size on coal burst is studied quantitatively.

The simulated results show that there is a critical in situ stress of unloading failure, which is about 0.7 times of UCS. When the initial in situ stress exceeds this critical value, the unloading can induce the failure of RCR. With the increase of the initial in situ stress, more AEs are generated in a shorter time and the unloading failure of RCR is more violent.

There is a critical surrounding rock stiffness, which is about 8.0 times the coal stiffness. When the surrounding rock stiffness is smaller than the critical value, a softer surrounding rock makes the unloading failure more violent. When the surrounding rock stiffness exceeds the critical value, the surrounding rock stiffness has almost no effect on the unloading failure.

The effective size of surrounding rock affecting the unloading failure is about 4.0 times the coal seam size. The surrounding rock outside the effective size has almost no effect on the unloading failure.

Acknowledgements This work is supported by the National Natural Science Foundation of China (Grant No. 11772190), which is gratefully acknowledged.

Declarations

Conflict of interest The authors declare that they have no competing interests.

References

- Chen H, Cheng Y, Zhou H, Li W (2013) Damage and permeability development in coal during unloading. *Rock Mech Rock Eng* 46: 1377–1390
- Gao H, Klein P (1998) Numerical simulation of crack growth in an isotropic solid with randomized internal cohesive bonds. *J Mech Phys Solids* 46(2):187–218
- Gong F, Wang Y, Wang Z, Pan J, Luo S (2021) A new criterion of coal burst proneness based on the residual elastic energy index. *Int J Min Sci Technol* (In Press)
- He M, Xia H, Jia X, Gong W, Zhao F, Liang K (2012) Studies on classification, criteria and control of rockbursts. *J Rock Mech Geotech Eng* 4(2):97–114
- He M, Ren F, Liu D, Zhang S (2021) Experimental study on strain burst characteristics of sandstone under true triaxial loading and double faces unloading in one direction. *Rock Mech Rock Eng* 54(1):149–171
- Liu J, Wang E, Song D, Wang S, Niu Y (2015) Effect of rock strength on failure mode and mechanical behavior of composite samples. *Arab J Geosci* 8:4527–4539
- Liu XS, Tan YL, Ning JG, Lu YW, Gu QH (2018) Mechanical properties and damage constitutive model of coal in coal-rock combined body. *Int J Rock Mech Min Sci* 110:140–150
- Lu J, Zhang D, Huang G, Li X, Gao H, Yin G (2020) Effects of loading rate on the compound dynamic disaster in deep underground coal mine under true triaxial stress. *Int J Rock Mech Min Sci* 134(10): 104453
- Manouchehrian A, Cai M (2016) Simulation of unstable rock failure under unloading conditions. *Can Geotech J* 53:22–34
- Si X, Gong F (2020) Strength-weakening effect and shear-tension failure mode transformation mechanism of rockburst for fine-grained granite under triaxial unloading compression. *Int J Rock Mech Min Sci* 131:104347
- Song Z, Konietzky H, Herbst M (2020) Drawing mechanism of fractured top coal in longwall top coal caving. *Int J Rock Mech Min Sci* 130:104329
- Song H, Zuo J, Liu H, Zuo S (2021) The strength characteristics and progressive failure mechanism of soft rock-coal combination samples with consideration given to interface effects. *Int J Rock Mech Min Sci* 138:104593
- Tao M, Li X, Wu C (2012) Characteristics of the unloading process of rocks under high initial stress. *Comput Geotech* 45:83–92
- Yao Q, Wang W, Zhu L, Xia Z, Tang C, Wang X (2020) Effects of moisture conditions on mechanical properties and AE and IR characteristics in coal-rock combinations. *Arab J Geosci* 13:615
- Yardimci AG, Karakus M (2020) A new protective destressing technique in underground hard coal mining. *Int J Rock Mech Min Sci* 130:104327
- Yin G, Jiang C, Wang JG, Xu J (2015) Geomechanical and flow properties of coal from loading axial stress and unloading confining pressure tests. *Int J Rock Mech Min Sci* 76:155–161
- Zhang Z (2013) Discretized virtual internal bond model for nonlinear elasticity. *Int J Solids Struct* 50:3618–3625
- Zhang M, Dou L, Konietzky H, Song Z, Huang S (2020) Cyclic fatigue characteristics of strong burst-prone coal: experimental insights

- from energy dissipation, hysteresis and micro-seismicity. *Int J Fatigue* 133:105429
- Zhou Z, Cai X, Li X, Cao W, Du X (2020) Dynamic response and energy evolution of sandstone under coupled static–dynamic compression: insights from experimental study into deep rock engineering applications. *Rock Mech Rock Eng* 53(3):1305–1331
- Zhu G, Dou L, Wang C, Ding Z, Feng Z, Xue F (2019) Experimental study of rock burst in coal samples under overstress and true-triaxial unloading through passive velocity tomography. *Saf Sci* 117:388–403
- Zuo J, Wang Z, Zhou H, Pei J, Liu J (2013) Failure behavior of a rock-coal-rock combined body with a weak coal interlayer. *Int J Min Sci Technol* 23:907–912